J Appl Electrochem (2012) 42:163–167
DOI 10.1007/s10800-012-0383-7

ORIGINAL PAPER

Three-dimensional lithium manganese phosphate microflowers for lithium-ion battery applications

P. Ramesh Kumar · M. Venkateswarlu · N. Satyanarayana

Received: 21 November 2011 / Accepted: 20 January 2012 / Published online: 2 February 2012

Abstract The Polyvinylpyrrolidone (PVP)-assisted polyol process was employed for the synthesis of lithium manganese phosphate ($LiMnPO_4$) microflowers as a cathode material for Li-ion battery applications. $LiMnPO_4$ microflowers were characterized by X-ray diffraction, scanning electron microscope, transmission electron microscope-energy dispersion spectroscope, and impedance spectroscopy. The microflowers were highly porous with nanosized petals. CR2032 coin cells were fabricated using $LiMnPO_4$ microflowers' sample and their battery characteristics were tested. The discharge capacity of $LiMnPO_4$ microflowers was found to be 164 mAh g^{-1} at 0.1C. The observed high discharge capacity was attributed to the short diffusion length of Li-ion motion in the nanopetals of the $LiMnPO_4$ microflowers.

Keywords Li-ion battery · $LiMnPO_4$ microflowers · Discharge capacity · Polyol process

1 Introduction

Lithium manganese phosphate is a potential cathode material for Li-ion batteries, as it is one of the compounds of the olivine structure [1–5]. In olivine structures, the three-dimensional (3D) framework is stabilized by the strong covalent bonds between oxygen ions and the P^{5+} resulting in PO_4^{3-} tetrahedral polyanions. As a result, the olivine type lithium metal phosphate materials are structurally stable during lithiation and de-lithiation. Lithium manganese phosphate has a redox potential of 4.1 V versus Li^+/Li. Therefore, to prepare the olivine-structured compounds in different shapes and sizes, researchers have investigated different synthesis methods like solid state reaction, hydrothermal, Sol–gel, polyol processes etc. [6–15]. The downside of $LiMnPO_4$ has low intrinsic electronic and ionic conductivity and poor discharge rate capability [14]. The electrochemical performance of $LiMnPO_4$ is poor especially at high current densities, which is attributed to the slow lithium-ion diffusion kinetics within the grains and the low intrinsic electronic conductivity [16, 17]. Well-known defects pairs, which hinder the lithium-ion diffusion in olivine structures includes Li/M antisite defects, M ion on a Li site, and lithium vacancy in olivine [18]. One of the best approaches to improve the performance rate of the olivine material is to develop nanosized particles in different shapes, which can reduce the diffusion path length for lithium-ions motion while creating a large contact area [19]. Further, improvement can also be undertaken through doping or coating of conductive additives, such as carbon, super ions doping, etc. This being the motivation behind our present study, an attempt to prepare 3D lithium manganese phosphate of marigold-type microflowers with nanopetals was successfully prepared by the polyvinylpyrrolidone (PVP)-assisted polyol process. The structural and microstructural properties of the $LiMnPO_4$ microflowers were investigated by XRD, SEM, TEM-EDS. Electrical properties of the $LiMnPO_4$ microflowers were studied using impedance spectroscopy. In addition, rechargeable lithium batteries of CR2032 type coin cells were fabricated using the newly-developed $LiMnPO_4$ microflowers with nanopetals and their electrochemical

P. Ramesh Kumar · N. Satyanarayana (✉)
Department of Physics, Pondicherry University, Pondicherry 605014, India
e-mail: nallanis2011@gmail.com

M. Venkateswarlu
Research and Development, Amara Raja Batteries, Tirupati 517501, Andhra Pradesh, India

properties were investigated through charge/discharge measurements.

2 Experimental

Lithium manganese phosphate microflowers were prepared by the PVP-assisted polyol process using AR grade (Sigma-Aldrich) chemicals such as Li-acetate, Mn-acetate, and ammonium dihydrogen phosphate. Stoichiometrically-calculated precursor chemicals were mixed in a double necked, round bottomed flask, and stirred at 190 °C for 3 h. In this process, PVP (PVP, M_w:360,000, Sigma-Aldrich, 1:2 weight ratio of $LiMnPO_4$:PVP) was used as a stabilizer to reduce the agglomeration as well as to control particle dimensions. Temperature, time of reaction and PVP concentration are very important in this PVP assisted polyol process as reaction conditions play significant role in obtaining the shape control of nanoparticles. The light gray colored $LiMnPO_4$ sample was obtained after washing the precipitate with acetone. The prepared sample was further heated up to 600 °C for 3 h. and the $LiMnPO_4$ microflowers were subsequently obtained.

The X-ray Diffractometer (XRD) from PANanlytical, Philips equipped with Cu-Kα radiation source ($\lambda =$ 1.5405 Å) was used for recording the XRD patterns of the $LiMnPO_4$ microflowers. The FTIR spectra were recorded on thin transparent pellet samples using Shimadzu FTIR/8300/8700 spectrophotometer in the range of 4,000–400 cm^{-1} with 2 cm^{-1} resolution for 20 scans. The Inspect S50 scanning electron microscopy (SEM) manufactured by FEI, Netherlands was used for imaging the microstructure of the prepared $LiMnPO_4$ microflowers. Transmission electron microscope with energy dispersive spectroscopy (TEM-EDS), JEOL 2010F HRTEM, Japan, with 200 kV operating voltage was used to capture the TEM images of the $LiMnPO_4$ sample. LiMnPO4 microflowers as a cathode material were used for the fabrication of lithium-ion batteries using CR2032 coin cells consisting 75 wt% of active cathode material, 15 wt% conductive carbon (Super P, Timcal USA), and 5 wt% of poly(vinylidene fluoride) (PVDF) used as a binder in N-methyl-2-pyrrolidone (NMP). Celgard 2340 micro-porous, three-layered polymer (poly propylene/polyethylene/polypropylene (PP/PE/PP)) membrane was used as a separator. 1 M $LiPF_6$ in ethylene carbonate: diethyl carbonate EC: DEC (1:1 v/v) was used as an electrolyte. A lithium metal was used (Aldrich) as the anode. The coin cells were assembled in a glove box filled with Argon gas. The charge/discharge cycles were galvanostatically performed at a current of 0.1C with cut-off voltages in range of 3.2–4.2 V (versus Li/Li^+) for 20 cycles at room temperature using multi-channel battery cycle tester (ARBIN BT2000, USA).

3 Results and discussion

The XRD pattern of the $LiMnPO_4$ microflowers sample along with the JCPDS data (No. 740375) is shown in Fig. 1. The observed XRD peaks were indexed to an orthorhombic crystal structure (space group *Pmnb*) of $LiMnPO_4$. The crystallite size (D) was calculated using the Scherrer Formula: $\beta \cos(\theta) = k\lambda/D$, where β is the full width-at-half-maximum length of the reflection. The calculated crystallite size of the pure $LiMnPO_4$ microflower with nanopetals sample was found to be 65 nm which shows that the prepared $LiMnPO_4$ sample is in the nanocrystalline phase.

The FTIR spectrum of the heated $LiMnPO_4$ microflowers sample is presented in Fig. 2. FTIR bands at 900 and 1,055 cm^{-1} are due to the symmetrical and the asymmetrical stretching of PO_4^{-3}. The presence of broad O–H band at 3,055 cm^{-1} is due to the hygroscopic nature of the sample while the IR band at 550 cm^{-1} was attributed

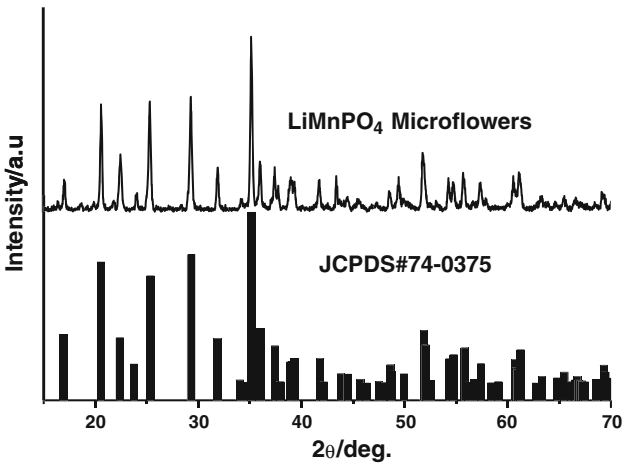

Fig. 1 XRD patterns of the $LiMnPO_4$ microflowers along with JCPDS data

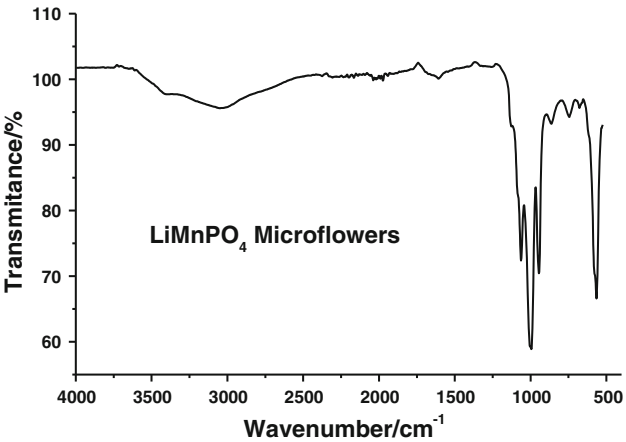

Fig. 2 FTIR spectrum for the $LiMnPO_4$ microflowers

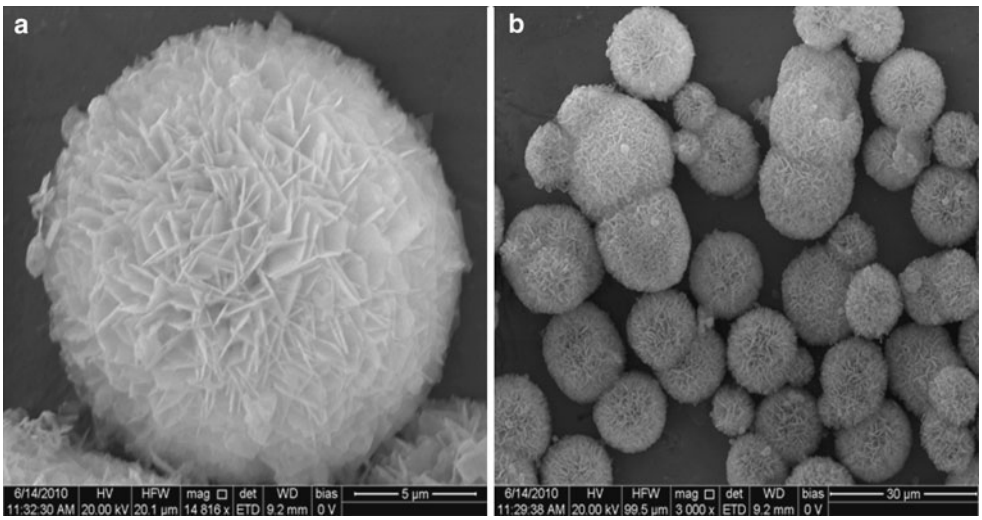

Fig. 3 SEM images of the $LiMnPO_4$ microflowers **a** single $LiMnPO_4$ microflower and **b** images with lower magnification

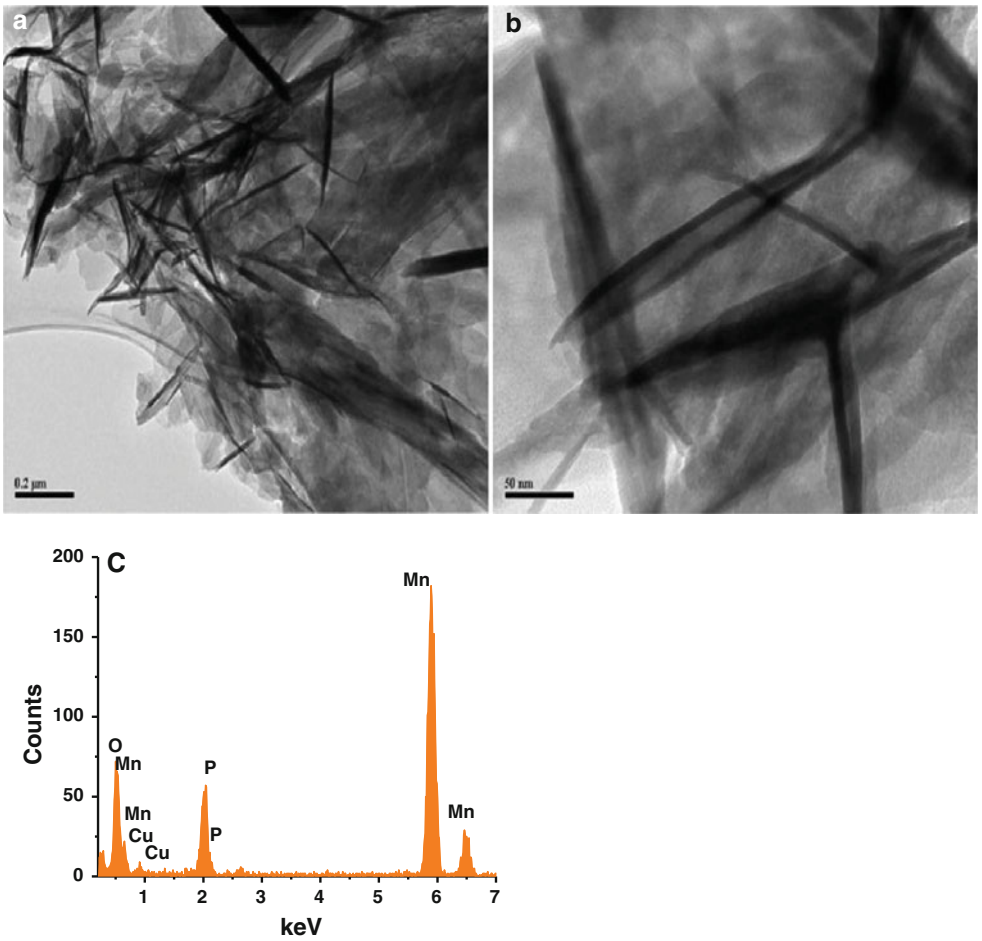

Fig. 4 **a**, **b** TEM images of the $LiMnPO_4$ microflower petals at different magnifications and **c** EDS spectrum of the $LiMnPO_4$ microflower petals

to the vibrations of PO_4^{-3}. Thus, FTIR results confirm the presence of PO_4^{-3} structure in the $LiMnPO_4$ microflowers.

Figure 3a shows the prepared $LiMnPO_4$ single marigold type of microflower with very thin petals and Fig. 3b shows the SEM images taken with lower magnification for the $LiMnPO_4$ marigold type microflowers. The SEM analysis indicated that the average size of the $LiMnPO_4$ marigold-type flowers was about 12 µm in diameter. The

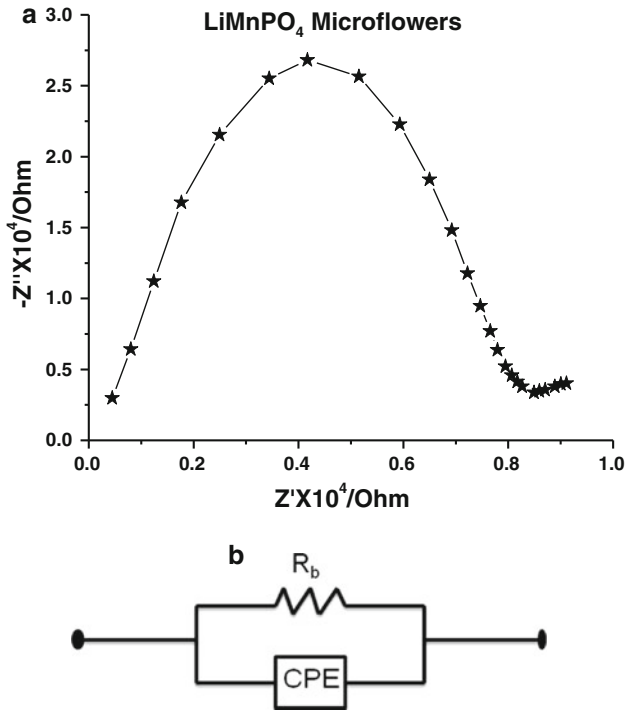

Fig. 5 **a** Impedance plots for the $LiMnPO_4$ microflowers sample at room temperature and **b** its equivalent circuit

TEM pictures and the EDS spectrum were taken for the well-sonicated $LiMnPO_4$ microflowers powder and the size of the microflowers' nanopetals were found to be ~10 nm in thickness. Figure 4a, b shows the TEM images of the petals of the $LiMnPO_4$ microflower with different magnifications. Figure 4c shows the EDS spectrum of the $LiMnPO_4$ microflowers from which the presence of Mn, P, and O elements were confirmed. The SEM and TEM-EDS support that the $LiMnPO_4$ marigold-type microflowers with nanopetals were successfully prepared using the PVP-assisted Polyol process.

Impedance plot at room temperature is given in Fig. 5a and the equivalent circuit for the $LiMnPO_4$ microflowers sample can be found in Fig. 5b. The intercept of the depressed semicircle at the real axis (*x*-axis) gives the best bulk resistance (R_b) for the sample and the intercept shifts toward the origin and the frequency at which the z'' attains a maximum shift toward higher frequencies as the temperature increases. The bulk resistance (R_b) was obtained from the fitted impedance data using winfit software and the pellet dimensions were used to calculate the bulk conductivity of the $LiMnPO_4$ microflowers samples measured at various temperatures [20].

Figure 6a shows the voltage versus the discharge capacity of $LiMnPO_4$ microflowers sample. The Li/$LiMnPO_4$ cell shows the flat lithium intercalation voltage curve at 4.1 V (Vs. Li). The discharge capacity of lithium-ion coin cells at 0.1C rate during the 1st cycle was observed as

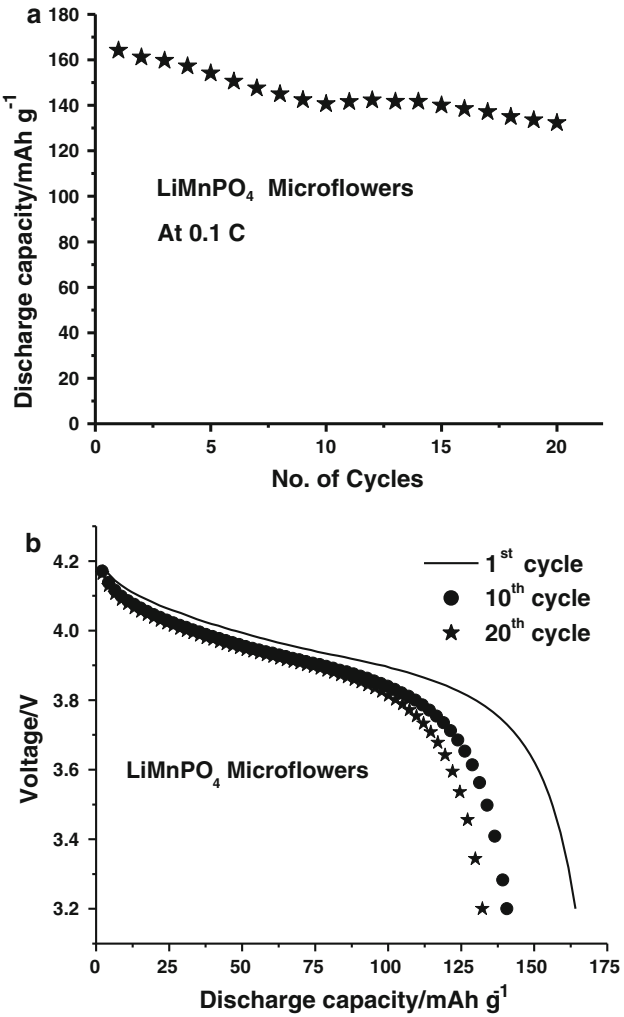

Fig. 6 **a** Discharge capacity versus number of cycles plot and **b** voltage versus discharge capacity plot for the $LiMnPO_4$ microflowers

164 mAh g^{-1}, while at the 20th cycle it was 132 mAh g^{-1}. The discharge capacity loss in the Li/$LiMnPO_4$ microflowers cell was around 20% between the 1st and the 20th cycles. It can be concluded that the prepared $LiMnPO_4$ microflowers with nanopetals have better capacity compared to other $LiMnPO_4$ particles reported by several researchers previously [7, 8, 13]. From the graph in Fig. 6b, it is also important to point out that the $LiMnPO_4$ microflowers showed less capacity fading. This might potentially be due to the Jahn–Teller distortion in the $MnPO_4$ after lithium deinsertion due to the Mn^{3+}, which has a high spin configuration [21, 22].

4 Conclusions

The 3D lithium manganese phosphate microflowers were successfully synthesized using the PVP-assisted Polyol

process. The phase, microstructure, and elemental analysis of the prepared $LiMnPO_4$ microflowers were confirmed by the XRD, SEM, and the TEM-EDS. The bulk conductivity of the $LiMnPO_4$ microflowers sample at room temperature was found to be 6.8×10^{-8} S cm^{-1}. The $LiMnPO_4$ microflowers with nanopetals were seen to have higher capacity and better cyclability than the earlier reported results with regard to the $LiMnPO_4$, which could possibly be due to the high surface area, defect-free and unidirectional ionic transportation in the nanopetals of $LiMnPO_4$ microflowers. The CR2032 coin cells were fabricated using the $LiMnPO_4$ microflowers sample and the charge/discharge characteristics voltage was found to be between 4.2 and 3.2 V and delivering maximum discharge capacity of 164 mAh g^{-1} at 0.1C. Hence, we suggest that the 3D lithium manganese phosphate microflowers sample is an important class of material in the development of next generation cathode materials for the Li-ion batteries.

Acknowledgments N.S. is grateful to DRDO, CSIR, AICTE, UGC, and DST, Government of India for providing financial support in the form of research projects.

References

1. Padhi AK, Nanjundaswamy K, Goodenough JB (1997) J Electrochem Soc 144:1188
2. Piana M, Arrabito M, Bodoardo S, D'Epifanio A, Satolli D, Croce F, Scrosati B (2002) Ionics 8:17
3. Zhou F, Kang K, Maxisch T, Ceder G, Morgan D (2004) Solid State Commun 132:181
4. Yamada A, Hosoya M, Chung SC, Kudo Y, Hinokuma K, Liu KY, Nishi Y (2003) J Power Sources 119–121:232
5. Yamada A, Chung SC (2001) J Electrochem Soc 148:A960
6. Li G, Azuma H, Tohda M (2002) Electrochem Solid State Lett 5:A135
7. Vadivel Murugan A, Muraliganth T, Ferreira PJ, Manthiram A (2009) Inorg Chem 48:946
8. Ramesh Kumar P, Venkateswarlu M, Misra M, Mohanty AK, Satyanarayana N (2011) J Electrochem Soc 158:A227
9. Morgan D, Van der Ven A, Ceder G (2004) Electrochem Solid-State Lett 7:A30
10. Chung SY, Chiang YM (2003) Electrochem Solid State Lett 6:A278
11. Bakenov Z, Taniguchi I (2010) Electrochem Commun 12:75
12. Kang B, Ceder G (2010) J Electrochem Soc 157:A808
13. Martha SK, Markovsky B, Grinblat J, Gofer Y, Haik O, Zinigrad E, Aurbach D, Drezen T, Wang D, Deghenghi G (2009) J Electrochem Soc 156:A541
14. Xiao J, Xu W, Choi D, Zhang J (2010) J Electrochem Soc 157:A142
15. Hu Y, Doeff MM, Kostecki R, Finones R (2004) J Electrochem Soc 151:A1279
16. Wang D, Wu X, Wang Z, Chen L (2005) J Power Sources 140:125
17. Takahashi M, Tobishima S, Takei K, Sakurai Y (2002) Solid State Ion 148:283
18. Fisher CAJ, Hart Prieto VM, Saiful Islam M (2008) Chem Mater 20:5907
19. Malik R, Burch D, Bazant M, Ceder G (2010) Nano Lett 10:4123
20. Bard AJ, Faulkner JR (2001) Electrochem methods, 2nd edn. Wiley, New York, p 231
21. Nie ZX, Ouyang CY, Chen JZ, Zhong ZY, Du YL, Liu DS, Shi SQ, Lei MS (2010) Solid State Commun 150:40
22. Choi D, Xiao J, Choi YJ, Hardy JS, Vijayakumar M, Liu J, Xu W, Wang W, Zhang JG, Graff GL, Yang Z (2011) Energy Environ Sci 4:4560